A&A 551, A67 (2013)
DOI: 10.1051/0004-6361/201220701

Astronomy & Astrophysics

Asteroids' physical models from combined dense and sparse photometry and scaling of the YORP effect by the observed obliquity distribution⋆

J. Hanuš[1], J. Ďurech[1], M. Brož[1], A. Marciniak[2], B. D. Warner[3], F. Pilcher[4], R. Stephens[5], R. Behrend[6], B. Carry[7], D. Čapek[8], P. Antonini[9], M. Audejean[10], K. Augustesen[11], E. Barbotin[12], P. Baudouin[13], A. Bayol[11], L. Bernasconi[14], W. Borczyk[2], J.-G. Bosch[15], E. Brochard[16], L. Brunetto[17], S. Casulli[18], A. Cazenave[12], S. Charbonnel[12], B. Christophe[19], F. Colas[20], J. Coloma[21], M. Conjat[22], W. Cooney[23], H. Correira[24], V. Cotrez[25], A. Coupier[11], R. Crippa[26], M. Cristofanelli[17], Ch. Dalmas[11], C. Danavaro[11], C. Demeautis[27], T. Droege[28], R. Durkee[29], N. Esseiva[30], M. Esteban[11], M. Fagas[2], G. Farroni[31], M. Fauvaud[12,32], S. Fauvaud[12,32], F. Del Freo[11], L. Garcia[11], S. Geier[33,34], C. Godon[11], K. Grangeon[11], H. Hamanowa[35], H. Hamanowa[35], N. Heck[20], S. Hellmich[36], D. Higgins[37], R. Hirsch[2], M. Husarik[38], T. Itkonen[39], O. Jade[11], K. Kamiński[2], P. Kankiewicz[40], A. Klotz[41,42], R. A. Koff[43], A. Kryszczyńska[2], T. Kwiatkowski[2], A. Laffont[11], A. Leroy[12], J. Lecacheux[44], Y. Leonie[11], C. Leyrat[44], F. Manzini[45], A. Martin[11], G. Masi[11], D. Matter[11], J. Michałowski[46], M. J. Michałowski[47], T. Michałowski[2], J. Michelet[48], R. Michelsen[11], E. Morelle[49], S. Mottola[36], R. Naves[50], J. Nomen[51], J. Oey[52], W. Ogłoza[53], A. Oksanen[49], D. Oszkiewicz[34,54], P. Pääkkönen[39], M. Paiella[11], H. Pallares[11], J. Paulo[11], M. Pavic[11], B. Payet[11], M. Polińska[2], D. Polishook[55], R. Poncy[56], Y. Revaz[57], C. Rinner[31], M. Rocca[11], A. Roche[11], D. Romeuf[11], R. Roy[58], H. Saguin[11], P. A. Salom[11], S. Sanchez[51], G. Santacana[12,30], T. Santana-Ros[2], J.-P. Sareyan[59,60], K. Sobkowiak[2], S. Sposetti[61], D. Starkey[62], R. Stoss[51], J. Strajnic[11], J.-P. Teng[63], B. Trégon[64,12], A. Vagnozzi[65], F. P. Velichko[66], N. Waelchli[67], K. Wagrez[11], and H. Wücher[30]

(Affiliations can be found after the references)

Received 5 November 2012 / Accepted 15 January 2013

ABSTRACT

Context. The larger number of models of asteroid shapes and their rotational states derived by the lightcurve inversion give us better insight into both the nature of individual objects and the whole asteroid population. With a larger statistical sample we can study the physical properties of asteroid populations, such as main-belt asteroids or individual asteroid families, in more detail. Shape models can also be used in combination with other types of observational data (IR, adaptive optics images, stellar occultations), e.g., to determine sizes and thermal properties.

Aims. We use all available photometric data of asteroids to derive their physical models by the lightcurve inversion method and compare the observed pole latitude distributions of all asteroids with known convex shape models with the simulated pole latitude distributions.

Methods. We used classical dense photometric lightcurves from several sources (Uppsala Asteroid Photometric Catalogue, Palomar Transient Factory survey, and from individual observers) and sparse-in-time photometry from the U.S. Naval Observatory in Flagstaff, Catalina Sky Survey, and La Palma surveys (IAU codes 689, 703, 950) in the lightcurve inversion method to determine asteroid convex models and their rotational states. We also extended a simple dynamical model for the spin evolution of asteroids used in our previous paper.

Results. We present 119 new asteroid models derived from combined dense and sparse-in-time photometry. We discuss the reliability of asteroid shape models derived only from Catalina Sky Survey data (IAU code 703) and present 20 such models. By using different values for a scaling parameter $c_{\rm YORP}$ (corresponds to the magnitude of the YORP momentum) in the dynamical model for the spin evolution and by comparing synthetic and observed pole-latitude distributions, we were able to constrain the typical values of the $c_{\rm YORP}$ parameter as between 0.05 and 0.6.

Key words. minor planets, asteroids: general

1. Introduction

The lightcurve inversion method (LI) was developed by Kaasalainen & Torppa (2001) and Kaasalainen et al. (2001). This powerful tool allows us to derive physical models of asteroids (their rotational states and the shapes) from series of disk-integrated photometry.

Convex asteroid shape models can be derived from two different types of disk-integrated photometry: dense or sparse-in-time. Originally, only dense photometry was used. About 20 such dense lightcurves from at least four or five apparitions are necessary for a unique shape determination. By this approach, ~100 asteroid models have been derived (e.g., Kaasalainen et al. 2002; Michałowski et al. 2004; Ďurech et al. 2007; Marciniak et al. 2007, 2008). To significantly enlarge the number of asteroid models, sparse photometric data were studied and used in the LI. Ďurech et al. (2009) determined 24 asteroid models from a combination of dense data with sparse photometry from the U.S. Naval Observatory in Flagstaff (USNO-Flagstaff station, IAU code 689). Sparse data from seven astrometric surveys (including USNO-Flagstaff station) were used in the LI by

⋆ Table 3 is available in electronic form at http://www.aanda.org

Hanuš et al. (2011), who presented 80 asteroid models. Sixteen models were based only on sparse data, the rest on combined dense and sparse data.

Models of asteroids derived by the lightcurve inversion method are stored in the Database of Asteroid Models from Inversion Techniques (DAMIT[1], Ďurech et al. 2010). In October 2012, models of 213 asteroids were included there.

A larger number of asteroids with derived models of their convex shapes and rotational states is important for further studies. Large statistical samples of physical parameters can tell us more about processes that take place in the asteroids' populations (near-Earth asteroids, main-belt asteroids, or asteroids in individual families). For example, an anisotropy of spin-axis directions is present in the population of main-belt asteroids with diameters $\lesssim$30 km (Hanuš et al. 2011), where the YORP effect[2], together with collisions and mass shedding, is believed to be responsible. There are similar effects on the rotational states of main-belt binaries (Pravec et al. 2012). Convex shape models were also used in combination with stellar occultations by asteroids where global nonconvexities can be detected, and the diameter can be estimated with a typical uncertainty of 10% (see Ďurech et al. 2011).

In Sect. 2, we describe the dense and sparse photometric data used in the lightcurve inversion method and present new asteroid models derived from combined photometric data sets or from the sparse-in-time data from the Catalina Sky Survey Observatory (IAU code 703) alone. The reliability tests for derived models are also described. In Sect. 3, we use a theoretical model of the latitude distribution of pole directions published in Hanuš et al. (2011) in a numerical simulation to constrain the free scaling parameter $c_{\rm YORP}$ describing our uncertainty in the shape and the magnitude of the YORP momentum.

2. Asteroid models

We used four main sources of dense photometric lightcurves: (i) the Uppsala Asteroid Photometric Catalogue (UAPC[3], Lagerkvist et al. 1987; Piironen et al. 2001), where lightcurves for about 1000 asteroids are stored; (ii) data from a group of individual observers provided via the Minor Planet Center in the Asteroid Lightcurve Data Exchange Format (ALCDEF[4], Warner et al. 2009); (iii) data from another group of individual observers available online via Courbes de rotation d'astéroïdes et de comètes (CdR[5]); and (iv) data from the Palomar Transient Factory survey (PTF[6], Rau et al. 2009). Polishook et al. (2012) recently analyzed a small fraction of PTF data and presented dense lightcurves for 624 asteroids. So far, only a fraction of photometric data from the PTF has been processed (four overlapping fields on four consecutive nights), which means that this source will become very important in the near future.

We downloaded sparse data from the AstDyS site (Asteroids – Dynamic Site[7]) and gathered sparse lightcurves from the USNO-Flagstaff station (IAU code 689) for ~1000 asteroids, from Roque de los Muchachos Observatory, La Palma (IAU code 950) for ~500 asteroids and $\gtrsim$100 sparse data points from the Catalina Sky Survey Observatory (CSS for short, IAU code 703, Larson et al. 2003) for ~4000 asteroids. We present 119 asteroid models derived from combined dense and sparse data (Sect. 2.2) and 20 models based only on CSS data (Sect. 2.3).

During the model computation, a priori information about the rotational period of the asteroid was used, which significantly reduced the volume of the multidimensional parameter space that had to be searched, and saved computational time. Period values were taken from the regularly updated Minor Planet Lightcurve Database[8] (Warner et al. 2009). If the period was unknown or insecure, we searched the model over all possible period values of 2–100 h (usually, when only sparse data are available).

2.1. Reliability tests

We carefully tested the reliability of derived models. If we had several dense lightcurves and sparse data from USNO-Flagstaff station for an asteroid, we considered a model as unique if: (i) the modeled sidereal rotational period was close to the synodic rotational period determined from a single apparition dense data set (synodic period values have usually been previously published and were available in the Minor Planet Lightcurve Database); (ii) the shape model rotated close to its axis with a maximum momentum of inertia (it was in a relaxed rotational state); and (iii) models with half and double period values gave significantly worse fits.

It was necessary to apply additional tests to models derived from sparse-in-time data alone. We used the tests presented in Hanuš et al. (2011, for more details, see Sect. 3.3 there), and they were sufficient if photometry from USNO-Flagstaff station was present. In Hanuš & Ďurech (2012), we have shown that reliable asteroid models can also be derived from the Catalina Sky Survey data alone, and we described a convenient procedure for how to proceed during the computation when the rotational period is unknown: the solution should be searched for all periods in an interval of 2–100 h, and the stability of the solution should be tested for at least two different shape parametrizations[9]. The correct solution had to be stable for both low ($n = 3$) and high ($n = 6$) shape resolutions. We followed these recommendations: we searched for the model in the multidimensional parameter space for shape resolutions $n = 3$ and $n = 6$ and checked that we derived solutions with similar rotational states. In Hanuš & Ďurech (2012), we tested values $n = 2, 3, 4, 5, 6$ for the shape resolution. Correct solutions (i.e., models from the CSS data were similar to the models based on different data sets) were reproduced for most values of n. On the other hand, incorrect solutions were derived only for values $n = 6$ and sometimes also for $n = 4$ or $n = 5$, but never for $n = 2$ or $n = 3$.

2.2. Models from combined dense and sparse data

The shape model determination scheme was very similar to the one used in Hanuš et al. (2011). 119 new asteroid models were

[1] http://astro.troja.mff.cuni.cz/projects/asteroids3D

[2] Yarkovsky–O'Keefe–Radzievskii–Paddack effect, a torque caused by the recoil force from anisotropic thermal emission, which can alter the rotational periods and orientation of spin axes, see e.g., Rubincam (2000), Vokrouhlický et al. (2003).

[3] http://asteroid.astro.helsinki.fi/

[4] http://www.minorplanet.info/alcdef.html

[5] http://obswww.unige.ch/~behrend/page2cou.html

[6] http://www.astro.caltech.edu/ptf/

[7] http://hamilton.dm.unipi.it/

[8] http://cfa-www.harvard.edu/iau/lists/LightcurveDat.html

[9] Shape is represented by coefficients of its expansion into spherical harmonic functions to the order n. We call n the shape resolution, the number of shape parameters is then $(n + 1)^2$, and our typical value for the shape resolution is $n = 6$.

derived because we gathered ~1000 new dense lightcurves from ALCDEF, another ~1000 lightcurves from PTF, ~300 from individual observers, and also additional sparse data observed by the CSS during the second half of the year 2010 and the first half of the year 2011. Derived rotational states with basic information about the photometry used for 119 asteroids are listed in Table 1. Out of them, 18 models are based only on *combined* sparse data from various sources, but in all cases, sparse data from USNO-Flagstaff station were present[10]. In Table 3, we list the references to the dense lightcurves we used for the new model determination.

Although the amount of photometric data from PTF was similar to that from ALCDEF, only two new shape models (for asteroids with numbers 52 820 and 57 394, see Table 1) were derived with their contribution. The first reason was a significantly worse quality of PTF data: only for 84 asteroids out of 624 were the data sufficient for determining a synodic period, while other lightcurves were noisy or burdened with systematic errors. In many cases they allowed only for an estimate of a lower limit for the lightcurve amplitude (presented in Polishook et al. 2012). The second reason was that PTF data alone were not sufficient for a unique model determination (they covered only one apparition), no other dense lightcurves were usually available, and sparse data were available for only fewer than a half of these asteroids. Many asteroids detected by the PTF survey were previously unknown.

There are previously published models available for 15 of the asteroids modeled here: (11) Parthenope, (79) Eurynome, (272) Antonia, (281) Lucretia, (351) Yrsa, (352) Gisela, (390) Alma, (787) Moskva, (852) Wladilena, (1089) Tama, (1188) Gothlandia, (1389) Onnie, (1572) Posnania, (1719) Jens, and (4954) Eric (see databases by Kryszczyńska et al. 2007; and Warner et al. 2009). As these models were usually based on limited datasets, our solutions differ from some of them substantially, while agreeing for some in the spin axis latitude or the sidereal period value. We fully confirmed previous models for six objects of that sample: the spin models of (79) Eurynome by Michałowski (1996), (787) Moskva by Svoren et al. (2009), and (1572) Posnania by Michałowski et al. (2001), as well as our preliminary solutions for (390) Alma, (1389) Onnie, and (1719) Jens obtained in Hanuš et al. (2011).

The shape models and their spin solutions can be found in the DAMIT database (Ďurech et al. 2010). We noticed that for the models based only on sparse data, their shapes tend to be very angular, with sharp edges and large planar areas, thus can be treated only as crude approximations of the real asteroid shapes. However, a substantial addition (≳10 lightcurves from ≳2 apparitions) of dense lightcurves smooths the shape models out, making them look more realistic, as confirmed by their better fit to occultation chords.

From observations of star occultations by asteroids, we can reconstruct asteroid projected silhouettes. These silhouettes can then be compared with the predicted contours of the convex shape models and used for the asteroid size determination by scaling the shape models to fit the occultation chords. A reasonable number of observations were available for three asteroids from our sample. By using the same methods as in Ďurech et al. (2011), we rejected mirror solutions for the asteroids (345) Tercidina and (578) Happelia, and also determined equivalent diameters (corresponding to spheres with the same volume as the scaled convex shape models): 96 ± 10 km for (345) Tercidina, 101 ± 5 km for (404) Arsinoe, and 70 ± 5 km for (578) Happelia. Two different stellar occultations are available for all three asteroids, and are plotted in Figs. 1–3.

During the apparition in 2004, the lightcurves of asteroid (1089) Tama have shown features typical of close binary systems (Behrend et al. 2004) and indeed, the system was later interpreted as a synchronous close binary (Behrend et al. 2006). Our *brick-like* convex shape model is strongly elongated with sharp edges and is similar to a convex shape model of a close binary system (90) Antiope. Such a shape appearance for close binaries was predicted from synthetic data (Ďurech & Kaasalainen 2003).

[10] Models based only on data from the Catalina Sky Survey are described later in Sect. 2.3.

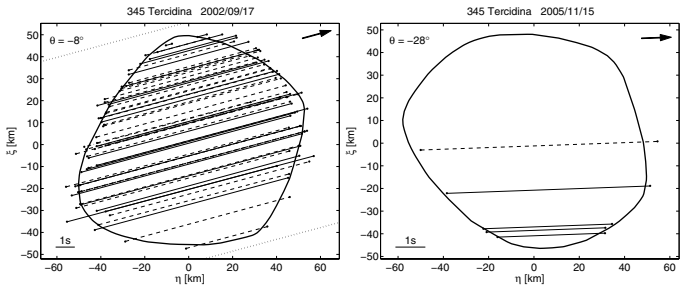

Fig. 1. Two observations of star occultations by asteroid (345) Tercidina. The solid contour corresponds to a scaled projected silhouette of the shape model with the pole (346°, −55°), each chord represents one occultation observation (solid lines are CCD, video, or photoelectric observations; dashed lines are visual observations, and dotted lines negative observations). Each plot also contains the time scale (lower left corner), the latitude of the sub-Earth point θ for the time of occultation (upper left corner), and the direction of the relative velocity (the arrow in the upper right corner). East points to the left and north up.

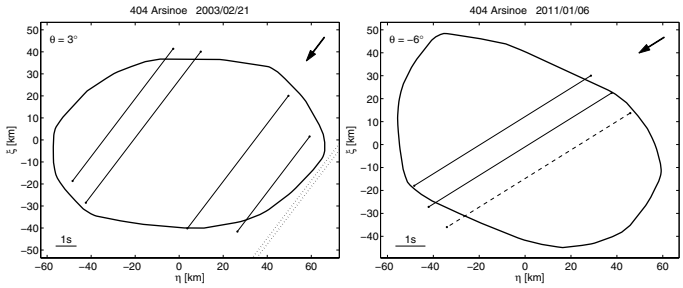

Fig. 2. Two observations of star occultations by asteroid (404) Arsinoe. The solid contour corresponds to a scaled projected silhouette of the shape model with the pole (25°, 57°). See Fig. 1 for line types and symbols explanation.

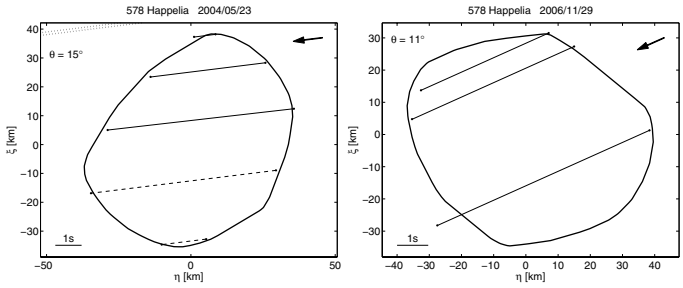

Fig. 3. Two observations of star occultations by asteroid (578) Happelia. The solid contour corresponds to a scaled projected silhouette of the shape model with the pole (339°, 62°). See Fig. 1 for line types and symbols explanation.

Table 1. List of new asteroid models derived from combined dense and sparse data or from sparse data alone.

Asteroid	λ_1 [deg]	β_1 [deg]	λ_2 [deg]	β_2 [deg]	P [h]	$N_{\rm lc}$	$N_{\rm app}$	N_{689}	N_{703}	N_{950}
11 Parthenope	311	14	128	14	13.72205	107	13	297	24	147
25 Phocaea	347	10			9.93540	22	5	272	100	
72 Feronia	287	−39	102	−55	8.09068	20	5	196	124	127
79 Eurynome	228	30	54	24	5.97772	36	4	240	168	
147 Protogeneia	269	15	90	14	7.85232	11	3	152	80	
149 Medusa	333	−73	156	−76	26.0454	13	4	134	60	
157 Dejanira	319	−64	146	−33	15.8287	14	2	94	123	
166 Rhodope	345	−22	173	−3	4.714793	7	2	141	111	
178 Belisana	260	20	79	9	12.32139	35	3	147	127	
183 Istria	85	20			11.76897	8	2	142	174	
193 Ambrosia	141	−11	328	−17	6.58166	18	4	169	87	
199 Byblis	344	−24	165	9	5.22063	22	5	184	108	
220 Stephania	26	−50	223	−62	18.2087	9	2	117	99	
222 Lucia	106	50	293	49	7.83671	9	4	160	100	
242 Kriemhild	100	−40	285	−15	4.545174	25	7	179	144	
257 Silesia	5	−53	176	−46	15.7097	18	2	167	88	
260 Huberta	23	−28	206	−19	8.29055	6	2	162	90	
265 Anna	109	−53			11.6903			114	79	
272 Antonia	293	−90			3.85480	7	2	109	92	
281 Lucretia	128	−49	309	−61	4.349711	8	4	129	83	
290 Bruna	286	−80	37	−74	13.8055	9	1	97	66	
297 Caecilia	223	−53	47	−33	4.151388	15	5	149	130	
345 Tercidina	346	−55			12.37082	42	8	161	155	
351 Yrsa	20	−70	193	−41	13.3120	2	1	183	52	
352 Gisela	24	−21	206	−28	7.48008	6	4	134	140	
371 Bohemia	93	49	256	43	10.73965	30	4	181	79	
390 Alma	53	−50	275	−76	3.74117	5	2	142	58	
403 Cyane	65	35	230	33	12.2700	7	3	186	104	
404 Arsinoe	25	57			8.88766	49	9	199	104	
406 Erna	357	−49	161	−60	8.79079	8	1	134	93	
441 Bathilde	285	55	122	43	10.44313	32	7	158	112	
507 Laodica	102	−55	312	−49	4.70657			162	103	
509 Iolanda	245	65	98	38	12.2907	4	2	178	85	
512 Taurinensis	324	45			5.58203	11	2	124	111	
519 Sylvania	106	9	286	−13	17.9647	5	2	147	76	
528 Rezia	176	−59	46	−66	7.33797	6	2	151	77	
531 Zerlina	78	−84			16.7073	28	3	48	52	
543 Charlotte	333	59	172	49	10.7184	4	1	138	98	
572 Rebekka	1	54	158	39	5.65009	5	2	155	63	
578 Happelia	339	62			10.06450	20	4	183	80	
600 Musa	0	−74	208	−46	5.88638	23	7	96	132	
669 Kypria	31	40	189	49	14.2789	5	1	142	126	
708 Raphaela	37	27	217	22	20.8894	5	1	140	95	
725 Amanda	145	−63	320	−70	3.74311	18	7	70	77	
731 Sorga	83	40	275	21	8.18633	7	2	131	136	
732 Tjilaki	160	23	353	24	12.3411	3	1	140	153	
787 Moskva	331	59	126	27	6.05581	15	4	160	92	
792 Metcalfia	88	−14	274	−13	9.17821	9	3	164	56	
803 Picka	218	34	53	41	5.07478			154	50	
807 Ceraskia	325	23	132	26	7.37390	2	1	132	111	
812 Adele	301	44	154	69	5.85746			65	119	
816 Juliana	124	−8	304	10	10.5627	11	2	158	107	
819 Barnardiana	169	46	334	47	66.698			121	86	
852 Wladilena	181	−48	46	−53	4.613301	30	8	138	101	
857 Glasenappia	227	48	38	34	8.20757	4	2	140	116	
867 Kovacia	200	−44	38	−50	8.67807			78	76	
874 Rotraut	201	−41	2	−36	14.3007	3	1	129	68	
875 Nymphe	42	31	196	42	12.6213	6	1	94	100	
900 Rosalinde	276	70	90	39	16.6868	3	2	125	170	
920 Rogeria	238	−15	47	−35	12.5749			137	79	

Notes. For each asteroid, the table gives the ecliptic coordinates λ_1 and β_1 of the pole solution with the lowest chi-square, the corresponding mirror solution λ_2 and β_2, the sidereal rotational period P, the number of dense lightcurves $N_{\rm lc}$ observed during $N_{\rm app}$ apparitions, and the number of sparse data points for the corresponding observatory: N_{689}, N_{703} and N_{950}. The uncertainty of the sidereal rotational period corresponds to the last decimal place of P and of the pole direction to 10–20°.

Table 1. continued.

Asteroid	λ_1 [deg]	β_1 [deg]	λ_2 [deg]	β_2 [deg]	P [h]	$N_{\rm lc}$	$N_{\rm app}$	N_{689}	N_{703}	N_{950}
958 Asplinda	41	48	226	35	25.3050	2	1	98	68	
994 Otthild	183	−50	41	–39	5.94819	26	5	140	125	
1040 Klumpkea	172	48			56.588			114	88	
1056 Azalea	252	51	64	41	15.0276	3	1	122	112	
1089 Tama	193	32	9	28	16.4461	90	7	108	79	
1111 Reinmuthia	356	68	153	78	4.007347	13	3	137	65	
1126 Otero	44	75	240	56	3.64800	2	1	101	110	
1130 Skuld	24	36	200	35	4.80764	14	1	92	106	
1188 Gothlandia	334	−84			3.491820	36	5	134	91	
1241 Dysona	125	−68			8.60738	7	1	156	64	
1249 Rutherfordia	32	74	197	65	18.2183	6	2	187	75	
1317 Silvretta	45	−57	161	−46	7.06797	13	3	120	69	
1386 Storeria	227	−67	297	−67	8.67795	10	1	33	78	
1389 Onnie	183	−75	0	−79	23.0447	2	1	90	97	
1393 Sofala	319	28	134	41	16.5931			69	91	
1401 Lavonne	204	23	27	44	3.93261	3	1	109	88	
1432 Ethiopia	41	44	225	54	9.84425	11	1	88	101	
1436 Salonta	223	18	57	35	8.86985	10	2	132	90	
1450 Raimonda	231	−56	71	−60	12.6344			74	116	
1472 Muonio	249	61	42	62	8.70543	6	1	99	93	
1490 Limpopo	319	22	142	2	6.65164	5	1	103	107	
1495 Helsinki	355	−39			5.33131	13	2	62	109	
1518 Rovaniemi	62	60	265	45	5.25047	2	1	100	73	
1528 Conrada	250	−51	93	−66	6.32154	2	1	93	126	
1554 Yugoslavia	281	−34	78	−64	3.88766	3	1	75	75	
1559 Kustaanheimo	275	29	94	33	4.30435			53	82	
1572 Posnania	205	−82	85	−63	8.04945	46	7	141	83	
1607 Mavis	0	59	222	70	6.14775	4	1	141	179	
1630 Milet	304	34	121	40	32.485	3	1	72	92	
1634 Ndola	261	45	66	34	64.255	7	1	71	110	
1704 Wachmann	267	41	90	40	3.31391			54	135	
1715 Salli	95	−24	254	−48	11.08867	2	1	84	97	
1719 Jens	286	−88	55	−42	5.87016	4	2	78	53	
1785 Wurm	11	57	192	47	3.26934	2	1	43	115	
1837 Osita	167	−64	352	−54	3.81879			82	62	
1905 Ambartsumian	52	−64	241	−68	92.153			50	101	
1927 Suvanto	74	73	278	23	8.16154	4	1	64	119	
1933 Tinchen	113	26	309	36	3.67062			72	103	
1950 Wempe	90	−41	258	−45	16.7953	1	1	96	46	
1963 Bezovec	219	7			18.1655	12	2	103	40	
1996 Adams	107	55			3.31114			82	120	
2002 Euler	30	44	188	47	5.99264	7	2		85	
2094 Magnitka	107	57	272	48	6.11219			25	84	
2510 Shandong	256	27	71	27	5.94639	4	1		132	
2606 Odessa	25	−81	283	−88	8.2444	3	1	25	129	
2709 Sagan	302	−14	124	−35	5.25636	6	2		160	
2839 Annette	341	−49	154	−36	10.4609	8	1		99	
2957 Tatsuo	81	45	248	32	6.82043	13	1	33	102	
2991 Bilbo	277	54	90	51	4.06175	3	1		97	
3722 Urata	260	−22	77	−9	5.5671	10	3		70	
4954 Eric	86	−54			12.05207	7	2		68	
5281 Lindstrom	238	−72	84	−81	9.2511	2	1		76	
7517 1989 AD	314	−60	123	−51	9.7094	4	1		81	
8132 Vitginzburg	33	−66	193	−48	7.27529	3	1		100	
8359 1989 WD	121	−68	274	−68	2.89103	6	1		105	
10772 1990 YM	16	46			68.82	5	1		73	
31383 1998 XJ_{94}	110	−74	279	−63	4.16818	4	1		71	
52820 1998 RS_2	228	−57	58	−48	2.13412	1	1		45	
57394 2001 RD_{84}	65	68	241	59	6.7199	4	1		47	

Table 2. List of new asteroid models derived from the Catalina Sky Survey data alone.

Asteroid	λ_1 [deg]	β_1 [deg]	λ_2 [deg]	β_2 [deg]	P [h]	N_{703}	$P_{\rm publ}$ [h]	Period reference
2112 Ulyanov	156	48	334	65	3.04071	118	3.000	Maleszewski & Clark (2004)
2384 Schulhof	196	−60	45	−42	3.29367	121	3.294	Ditteon et al. (2002)
2617 Jiangxi	224	76	1	54	11.7730	124	11.79	Carbo et al. (2009)
3170 Dzhanibekov	217	60	21	64	6.07168	105	6.0724	Molnar et al. (2008)
4507 1990 FV	143	55	323	49	6.57933	84	6.58	Yoshida et al. (2005)
5647 1990 TZ	253	77	119	−19	6.13867	87	6.144	Bembrick & Bolt (2003)
10826 1993 SK_{16}	260	−56	60	−34	13.8327	90	13.835	Galad (2008)
19848 Yeungchuchiu	190	−68			3.45104	104	3.450	Yeung (2006)
3097 Tacitus	229	71	72	62	8.7759	99		
4611 Vulkaneifel	5	−86	197	−50	3.75635	148		
5461 Autumn	249	−26	79	−43	20.0929	106		
5625 1991 AO_2	265	−52	97	−78	6.67411	110		
5960 Wakkanai	226	−69	69	−61	4.96286	102		
7201 Kuritariku	22	67	249	64	48.849	103		
7632 Stanislav	234	−50	46	−45	5.29073	99		
7905 Juzoitami	105	−76	226	−55	2.72744	118		
13002 1982 BJ_{13}	58	−50	245	−57	3.13844	110		
16009 1999 CM_8	283	44			8.3476	124		
16847 Sanpoloamosciano	91	−24			8.1845	114		
26792 1975 LY	226	68			79.15	140		

Notes. For each asteroid, the table gives the ecliptic coordinates λ_1 and β_1 of the pole solution, the corresponding mirror solution λ_2 and β_2, the sidereal rotational period P, the number of sparse data points from the CSS N_{703}, and the previously published period value $P_{\rm publ}$ with the reference. The uncertainty of the sidereal rotational period corresponds to the last decimal place of P and of the pole direction to 20–40°.

2.3. Models based on data from the Catalina Sky Survey astrometric project

There are two different groups of asteroid models based on CSS data: (i) models with previously reported synodic periods determined from dense data (we did not have these dense data, so period values were taken from the literature, usually from the Minor Planet Lightcurve Database); and (ii) models with previously unknown rotational periods. In the first case, we could compare the published period value with the period value derived by the LI (see Table 2, Cols. 7 and 9). If both periods agreed within their uncertainties, we considered the solution reliable. This test could not be performed for the second group of models, so we had to use additional reliability tests (see Sect. 2.1).

In Table 2, we present 20 asteroid models based only on the CSS data. The previous period estimates were not available for 12 of them. All of these 20 models have higher uncertainties of the pole orientations and lower shape resolution than models based on combined data, and all are possible candidates for follow-up lightcurve observations for period confirmation and more detailed shape determination.

3. Semi-empirical scaling of the YORP effect

Our enlarged sample of physical parameters for ~330 asteroids[11] validates our previous results based on a smaller asteroid sample (220 asteroids) presented in Hanuš et al. (2011). In Fig. 4, we show the observed *debiased* (i.e., we removed the systematic effect of the lightcurve inversion method caused by the method having a higher probability of deriving a unique solution for asteroids with larger pole latitudes. The debiasing procedure was based on a numerical simulation presented in Hanuš et al. 2011, see Sect. 4.3 there) latitude distributions of pole directions for main-belt asteroids with diameters $D < 30$ km and $D > 60$ km. The population of larger asteroids ($D > 60$ km) exhibits an excess of prograde rotators, probably of primordial origin (predicted also from numerical simulations by Johansen & Lacerda 2010). On the other hand, smaller asteroids ($D < 30$ km) have a clearly bimodal latitude distribution – most of the asteroids have ecliptic pole latitudes > 53°.

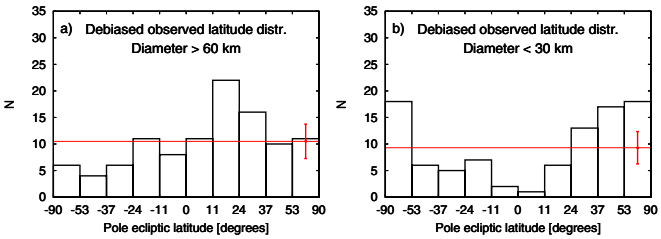

Fig. 4. Debiased observed latitude distribution of main-belt asteroids with diameters $D > 60$ km (*left panel*) and $D < 30$ km (*right panel*). The latitude bins are equidistant in $\sin\beta$. The thin horizontal line corresponds to the average value $\bar{N}$ and the errorbar to $\sqrt{\bar{N}}$.

The debiased observed latitude distribution of the pole directions of MBAs represents fingerprints from the past evolution of this population. Direct comparison between the observed asteroid properties and predictions of theoretical models can validate/exclude some of the asteroid dynamical evolution theories or constrain specific free parameters.

In Hanuš et al. (2011), we introduced a simple dynamical model for the spin evolution of asteroids, where we included (i) the YORP thermal effect; (ii) random reorientations induced by noncatastrophic collisions; (iii) oscillations caused by gravitational torques and spin-orbital resonances; and also (iv) mass shedding when a critical rotational frequency is reached. Because we studied a large statistical sample of

[11] According to the asteroid size distribution function of Davis et al. (2002), we have in our sample ~30% of all asteroids with $D > 100$ km, ~15% asteroids with 60 km < D < 100 km, and ~14% asteroids with 30 km < D < 60 km.

asteroids, the effect on the overall latitude distribution of pole directions caused by other processes (gravitational torques by the Sun, damping, or tumbling) was assumed to be only minor.

The model was based on the relations for the rate of the angular velocity ω ($\omega = 2\pi/P$) and the obliquity ϵ (Euler equations)

$$\frac{\mathrm{d}\omega}{\mathrm{d}t} = c f_i(\epsilon), \qquad i = 1 \ldots 200, \tag{1}$$

$$\frac{\mathrm{d}\epsilon}{\mathrm{d}t} = \frac{c g_i(\epsilon)}{\omega}, \tag{2}$$

where f- and g-functions describing the YORP effect for a set of 200 shapes with the effective radius $R_0 = 1$ km, the bulk density $\rho_0 = 2500\,\mathrm{kg/m^3}$, located on a circular orbit with the semi-major axis $a_0 = 2.5$ AU, were calculated numerically by Čapek & Vokrouhlický (2004). We assigned one of the artificial shapes (denoted by the index i) for each individual asteroid from our sample[12]. The f- and g-functions were scaled by a factor

$$c = c_{\mathrm{YORP}} \left(\frac{a}{a_0}\right)^{-2} \left(\frac{R}{R_0}\right)^{-2} \left(\frac{\rho_{\mathrm{bulk}}}{\rho_0}\right)^{-1}, \tag{3}$$

where a, R, ρ_{bulk} denote the semi-major axis, the radius, and the density of the simulated body, respectively, and c_{YORP} is a *free* scaling parameter reflecting our uncertainty in the shape models and the magnitude of the YORP torque, which dependents on small-sized surface features (even boulders, Statler 2009) and other simplifications in the modeling of the YORP torque.

We enhanced the simulation of the spin evolution of asteroids presented in Hanuš et al. (2011), by testing different values of the free parameter c_{YORP} and comparing the resulting synthetic latitude distributions with the observed debiased latitude distributions. Thanks to the new asteroid models, we had an updated observed spin vector distribution. We added 50% more observed asteroids, so we used 307 instead of 220 models for this comparison.

We used the following values of the parameter c_{YORP}: 0.01, 0.05, 0.1, 0.2, 0.3, 0.4, 0.5, 0.6, 0.8. Values of $c_{\mathrm{YORP}} \gtrsim 1$ were already recognized as unrealistic.

For each value of c_{YORP}, we ran 100 simulations with different random seeds to generate different initial ω and spin vector distributions. We integrated Eqs. (1) and (2) numerically. The time span was 4 Gyr with the time step of the explicit Euler scheme $\Delta t = 10$ Myr. As initial conditions, we assumed a Maxwellian distribution of angular velocities ω and isotropically distributed spin vectors. We also used $K = 10^{-2}\,\mathrm{W/K/m}$, $\rho_{\mathrm{bulk}} = 2500\,\mathrm{kg/m^3}$.

Every time a critical angular velocity ($\omega_{\mathrm{crit}} = \sqrt{4/3\pi G\rho_{\mathrm{bulk}}}$) was reached for an asteroid, we assumed a mass shedding event, so that we reset the rotational period to a random value from an interval of 2.5, 9 h. We altered the assigned shape, but we kept the sense of the rotation and the orientation of the spin axis. We also included a simple Monte-Carlo model for the spin axis reorientations caused by collisions (with $\tau_{\mathrm{reor}} = B\left(\frac{\omega}{\omega_0}\right)^{\beta_1}\left(\frac{D}{D_0}\right)^{\beta_2}$, where $B = 84.5\,\mathrm{kyr}$, $\beta_1 = 5/6$, $\beta_2 = 4/3$, $D_0 = 2\,\mathrm{m}$, and ω_0 corresponds to period $P = 5$ h, Farinella et al. 1998). After the collision, we reset the spin axis and period to random values (new period was from an interval of 2.5, 9 h). Collisional disruptions are not important in our case so they were not considered.

[12] We did not use the convex-hull shape models derived in this work because the two samples of shapes are believed to be statistically equivalent, and moreover, the YORP effect seems sensitive to small-scale surface structure (Scheeres & Mirrahimi 2007), which cannot be caught by our shape models.

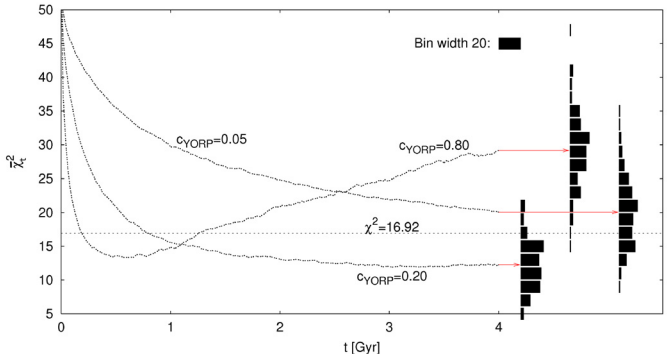

Fig. 5. Temporal evolution of the χ^2 that corresponds to the difference between the simulated latitude distributions, averaged over all 100 runs, and the debiased observed latitude distribution (i.e., $\bar{\chi}^2_t$) for three different values of parameter $c_{\mathrm{YORP}} = 0.05$, 0.20, and 0.80 (we performed a chi-square test). Vertical histograms on the righthand side represent the distributions of χ^2_{tj} at time $t = 4$ Gy for all 100 runs. Dotted line: the statistically significant probability value of 5%, i.e. $\chi^2 = 16.92$.

We also accounted for spin-orbital resonances by adding a sinusoidal oscillation to β (to prograde rotators, only, Vokrouhlický et al. 2006b) with a random phase and an amplitude $\simeq 40°$.

The spin states of our synthetic asteroids evolve during the simulation. At each time t of the simulation, we can construct a latitude distribution of the pole directions with the latitude values split into ten bins with a variable width corresponding to constant surface on the celestial sphere. Because we used ecliptic coordinates with the longitude λ and the latitude β, the bins were equidistant in $\sin\beta$. To describe the temporal evolution of the simulated latitude distributions, we computed a χ^2 metric between the simulated and the debiased observed latitude distributions of asteroids with diameters $D < 60$ km. The assumption of isotropically distributed initial spin vectors is not fulfilled for larger asteroids ($D > 60$ km), because this population has an excess of prograde rotators (see Fig. 4), which is believed to have a primordial origin (Johansen & Lacerda 2010). The second reason we rejected asteroids with $D > 60$ km from latitude comparison is that their evolution is rather slow compared to the simulation time span.

For each time t within the simulation run j ($j = 1 \ldots 100$), the corresponding chi-square value χ^2_{tj} is defined by

$$\chi^2_{tj} \equiv \sum_i \frac{(S_{tji} - O_i)^2}{\sigma^2_{tji}}, \tag{4}$$

where S_{tji} denotes the number of synthetic bodies with latitudes in bin i, O_i the number of observed latitudes in bin i, and $\sigma_{tji} \equiv \sqrt{S_{tji} + O_i}$ corresponds to the uncertainty estimate.

In Fig. 5, we show the temporal evolution of the *average* chi-square $\bar{\chi}^2_t = \sum_j \chi^2_{tj}/100$ in the course of our numerical simulations for different c_{YORP} values. As we see in Fig. 5, the average synthetic latitude distribution evolves in course of the time (while the debiased observed latitude distribution is fixed). We can distinguish three basic cases of the temporal evolution:

– When the YORP effect is weak ($c_{\mathrm{YORP}} \lesssim 0.1$), the synthetic latitude distribution only evolves slowly and is never similar to the observed latitude distribution, even at the end of the simulation, because $\bar{\chi}^2_t$ is still large (for $N = 9$, a statistically significant probability value of 5% corresponds to $\chi^2 = 16.92$).

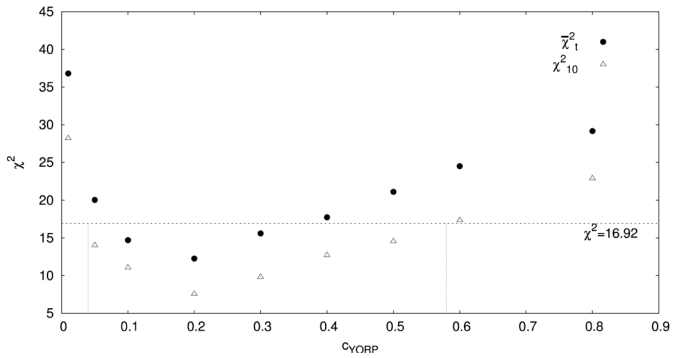

Fig. 6. Dependence of $\bar{\chi}^2_t$ and χ^2_{10} values calculated for the time t = 4 Gyr (i.e. the final state of the simulation) on different values of the c_{YORP} parameter. We also plotted the statistically significant probability value of 5% which corresponds to χ^2 = 16.92 and the interval of plausible c_{YORP} values from 0.05 to 0.6.

- A steady state (i.e., the state when the synthetic latitude distribution does not significantly evolve in time, and thus the $\bar{\chi}^2_t$ is approximately constant) is only reached for c_{YORP} values close to 0.2.
- For values $c_{YORP} \gtrsim 0.3$, the synthetic latitude distribution evolves faster and, at a certain time, is most similar to the observed latitude distribution (i.e., the minimum of $\bar{\chi}^2_t$). After that, the $\bar{\chi}^2_t$ grows, because the YORP significantly develops also larger asteroids, and thus the bins with low latitudes are depopulated more than is observed.

Vertical histograms on the righthand side of Fig. 5 represent the distributions of χ^2_{tj} at the time t = 4 Gy for all 100 runs. The average chi-square $\bar{\chi}^2_t$ of the model with c_{YORP} = 0.05 is substantially higher than 16.92, so this model can be considered wrong. However, from the distributions of χ^2_{tj} we can see that about 25% of individual runs have χ^2_{tj} lower than 16.92. To avoid rejecting those c_{YORP} values that are partially compatible with the observations, we should instead use a more representative value of χ^2 than the average $\bar{\chi}^2_t$, namely a value χ^2_{10}, for which 10% runs have lower χ^2_{tj} (see Fig. 6). Based on the χ^2_{10}, the most probable values of the c_{YORP} parameter are between 0.05 and 0.6.

4. Discusion and conclusions

Our preferred interpretation of the optimal c_{YORP} value being much lower than one is that small-scale features (boulders) tend to decrease the YORP torque. This hypothesis is supported by the independent modeling of Rozitis & Green (2012), who estimate, by including rough surface thermal-infrared beaming effects in their long-term spin evolution model, that the surface roughness is on average responsible for damping the magnitude of the YORP effect typically by half of the smooth surface predictions. This would correspond to c_{YORP} = 0.5 in our notation. The YORP effect is sensitive to the sizes of the boulders and can vary tens of percent, so the results of Rozitis & Green (2012) agree with our model.

As an important application, we mention that the constraint for the value of c_{YORP} can be used in simulations of the long-term dynamical evolution of asteroid families. So far, c_{YORP} has been used as a free parameter (e.g., in the method presented by Vokrouhlický et al. 2006a). Constraining c_{YORP} therefore *removes* one free parameter from the simulations and should thus lead to a better determination of the ages of asteroid families.

Finally, the results of this paper can be briefly summarized as follows.

- For 119 asteroids, we derived the convex shape models and rotational states from their combined disk-integrated dense and sparse photometric data. This effort was achieved with the help of ∼100 individual observers who were willing to share their lightcurves. The typical uncertainty of the sidereal rotational period is $\sim 10^{-5}$ h and of the pole direction 10–20°. All new models are now included in the DAMIT database.
- We also derived 20 asteroid models based purely on sparse-in-time photometry from the Catalina Sky Survey Observatory. The reliability of these models is supported by the fact that for eight of them, we obtained similar rotational period values that were previously reported in the literature and derived from an independent data set (dense photometry). We do not have any previous information about the rotational periods for the 12 other asteroids. Due to relatively larger uncertainties of the CSS sparse data, the typical uncertainty of the sidereal rotational period is $\sim 10^{-4}$–10^{-5} h and of the pole direction 20–40°.
- By combining observations of stellar occultations by asteroids with derived convex shape models, we determined equivalent diameters for the asteroids (345) Tercidina, (404) Arcinoe, and (578) Happelia to 96 ± 10 km, 101 ± 5 km, and 70 ± 5 km, respectively.
- We updated a simple dynamical model for the spin evolution of asteroids and compared the synthetic pole latitude distributions to the debiased observed latitude distributions of 307 asteroids. By using several values of the scaling parameter c_{YORP} defined by Eq. (3) (from 0.01 to 0.8), we constrained its value to $c_{YORP} \in [0.05, 0.6]$. We interpreted the low value of c_{YORP} as a result of the surface roughness.

Acknowledgements. The work of JH has been supported by grant GA UK 134710 of the Grant agency of the Charles University and by the project SVV 265301 of the Charles University in Prague. The work of J.H. and J.Ď. has been supported by grants GACR 209/10/0537 and P209/12/0229 of the Czech Science Foundation, the work of J.D. and M.B. by the Research Program MSM0021620860 of the Czech Ministry of Education, and the work of MB also by the grant GACR 13-01308S of the Grant Agency of the Czech Republic. The work of TSR was carried out through the Gaia Research for European Astronomy Training (GREAT-ITN) network. He has received funding from the European Union Seventh Framework Program (FP7/2007-2013) under grant agreement no. 264895. This work is partially based on observations made at the South African Astronomical Observatory (SAAO). It was based on observations made with the Nordic Optical Telescope, operated on the island of La Palma jointly by Denmark, Finland, Iceland, Norway, and Sweden, in the Spanish Observatorio del Roque de los Muchachos of the Instituto de Astrofisica de Canarias. This work is partially based on observations carried out with the Pic du Midi Observatory 0.6 m telescope, a facility operated by the Observatoire Midi-Pyrénées and Association T60, an amateur association. The calculations were performed on the computational cluster Tiger at the Astronomical Institute of Charles University in Prague (http://sirrah.troja.mff.cuni.cz/tiger).

References

Baker, R. E., Pilcher, F., & Klinglesmith III, D. A. 2012, Minor Planet Bulletin, 39, 60
Behrend, R., Roy, R., Rinner, C., et al. 2004, IAU Circ., 8265, 2
Behrend, R., Bernasconi, L., Roy, R., et al. 2006, A&A, 446, 1177
Bembrick, C., & Bolt, G. 2003, Minor Planet Bulletin, 30, 42
Bembrick, C., Crawford, G., Oey, J., & Allen, B. 2007, Minor Planet Bulletin, 34, 67
Brinsfield, J. W. 2008a, Minor Planet Bulletin, 35, 179
Brinsfield, J. W. 2008b, Minor Planet Bulletin, 35, 86
Brinsfield, J. W. 2009, Minor Planet Bulletin, 36, 169
Buchheim, R. K. 2005, Minor Planet Bulletin, 32, 35
Buchheim, R. K. 2007, Minor Planet Bulletin, 34, 68

Buchheim, R. K. 2010, Minor Planet Bulletin, 37, 41
Buchheim, R. K., Conjat, M., Roy, R., Baudoin, P., & Behrend, R. 2004, Minor Planet Bulletin, 31, 90
Čapek, D., & Vokrouhlický, D. 2004, Icarus, 172, 526
Carbo, L., Kragh, K., Krotz, J., et al. 2009, Minor Planet Bulletin, 36, 91
Davis, D. R., Durda, D. D., Marzari, F., Campo Bagatin, A., & Gil-Hutton, R. 2002, Asteroids III, 545
Ditteon, R., Bixby, A. R., Sarros, A. M., & Waters, C. T. 2002, Minor Planet Bulletin, 29, 69
Ďurech, J., & Kaasalainen, M. 2003, A&A, 404, 709
Ďurech, J., Scheirich, P., Kaasalainen, M., et al. 2007, in IAU Symp., 236, eds. G. B. Valsecchi, D. Vokrouhlický, & A. Milani, 191
Ďurech, J., Kaasalainen, M., Warner, B. D., et al. 2009, A&A, 493, 291
Ďurech, J., Sidorin, V., & Kaasalainen, M. 2010, A&A, 513, A46
Ďurech, J., Kaasalainen, M., Herald, D., et al. 2011, Icarus, 214, 652
Farinella, P., Vokrouhlicky, D., & Hartmann, W. K. 1998, Icarus, 132, 378
Galad, A. 2008, Minor Planet Bulletin, 35, 128
Hanuš, J., & Ďurech, J. 2012, Planet. Space Sci., 73, 75
Hanuš, J., Ďurech, J., Brož, M., et al. 2011, A&A, 530, A134
Higgins, D. 2008, Minor Planet Bulletin, 35, 30
Higgins, D., & Goncalves, R. M. D. 2007, Minor Planet Bulletin, 34, 16
Higgins, D., & Warner, B. D. 2009, Minor Planet Bulletin, 36, 159
Higgins, D., Pravec, P., Kusnirak, P., et al. 2006, Minor Planet Bulletin, 33, 89
Higgins, D., Pravec, P., Kusnirak, P., et al. 2008, Minor Planet Bulletin, 35, 123
Johansen, A., & Lacerda, P. 2010, MNRAS, 404, 475
Kaasalainen, M., & Torppa, J. 2001, Icarus, 153, 24
Kaasalainen, M., Torppa, J., & Muinonen, K. 2001, Icarus, 153, 37
Kaasalainen, M., Torppa, J., & Piironen, J. 2002, Icarus, 159, 369
Koff, R. A., & Brincat, S. M. 2000, Minor Planet Bulletin, 27, 49
Kryszczyńska, A., La Spina, A., Paolicchi, P., et al. 2007, Icarus, 192, 223
Lagerkvist, C., Barucci, M. A., Capria, M. T., et al. 1987, Asteroid photometric catalogue, eds. C.-I. Lagerkvist, M. A. Barucci, M. T. Capria, et al.
Larson, S., Beshore, E., Hill, R., et al. 2003, in BAAS, 35, AAS/Division for Planetary Sciences Meeting Abstracts #35, 982
López-González, M. J., & Rodríguez, E. 2000, A&AS, 145, 255
Maleszewski, C., & Clark, M. 2004, Minor Planet Bulletin, 31, 93
Marciniak, A., Michałowski, T., Kaasalainen, M., et al. 2007, A&A, 473, 633
Marciniak, A., Michałowski, T., Kaasalainen, M., et al. 2008, A&A, 478, 559
Michałowski, T. 1996, Icarus, 123, 456
Michałowski, T., Pych, W., Kwiatkowski, T., et al. 2001, A&A, 371, 748
Michałowski, T., Kwiatkowski, T., Kaasalainen, M., et al. 2004, A&A, 416, 353
Molnar, L. A., Haegert, J. M., Beaumont, C. N., et al. 2008, Minor Planet Bulletin, 35, 9
Oey, J. 2008, Minor Planet Bulletin, 35, 132
Oey, J. 2009, Minor Planet Bulletin, 36, 4
Oey, J., & Krajewski, R. 2008, Minor Planet Bulletin, 35, 47
Oey, J., Behrend, R., Pravec, P., et al. 2007, Minor Planet Bulletin, 34, 2
Piironen, J., Lagerkvist, C., Torppa, J., Kaasalainen, M., & Warner, B. 2001, in BAAS, 33, 1562
Pilcher, F. 2008, Minor Planet Bulletin, 35, 135
Pilcher, F. 2009a, Minor Planet Bulletin, 36, 133
Pilcher, F. 2009b, Minor Planet Bulletin, 36, 25
Pilcher, F. 2009c, Minor Planet Bulletin, 36, 100
Pilcher, F. 2010, Minor Planet Bulletin, 37, 119
Pilcher, F. 2011a, Minor Planet Bulletin, 38, 183
Pilcher, F. 2011b, Minor Planet Bulletin, 38, 76
Pilcher, F., & Brinsfield, J. W. 2011, Minor Planet Bulletin, 38, 206
Pilcher, F., Benishek, V., & Oey, J. 2009, Minor Planet Bulletin, 36, 68
Polishook, D. 2012, Minor Planet Bulletin, 39, 242
Polishook, D., & Brosch, N. 2008, Icarus, 194, 111
Polishook, D., & Brosch, N. 2009, Icarus, 199, 319
Polishook, D., Ofek, E. O., Waszczak, A., et al. 2012, MNRAS, 421, 2094
Pravec, P., Scheirich, P., Vokrouhlický, D., et al. 2012, Icarus, 218, 125
Rau, A., Kulkarni, S. R., Law, N. M., et al. 2009, PASP, 121, 1334
Rozitis, B., & Green, S. F. 2012, MNRAS, 423, 367
Rubincam, D. P. 2000, Icarus, 148, 2
Ruthroff, J. C. 2010, Minor Planet Bulletin, 37, 102
Scheeres, D. J., & Mirrahimi, S. 2007, in BAAS, 38, 416
Statler, T. S. 2009, Icarus, 202, 502
Stephens, R. D. 2005a, Minor Planet Bulletin, 32, 82
Stephens, R. D. 2005b, Minor Planet Bulletin, 32, 2
Stephens, R. D. 2008, Minor Planet Bulletin, 35, 126
Stephens, R. D. 2009a, Minor Planet Bulletin, 36, 59
Stephens, R. D. 2009b, Minor Planet Bulletin, 36, 18
Svoren, J., Husarik, M., Ambroz, J., Drbohlav, J., & Medek, J. 2009, Earth Moon and Planets, 105, 361
Vokrouhlický, D., Brož, M., Morbidelli, A., et al. 2006a, Icarus, 182, 92
Vokrouhlický, D., Nesvorný, D., & Bottke, W. F. 2003, Nature, 425, 147
Vokrouhlický, D., Nesvorný, D., & Bottke, W. F. 2006b, Icarus, 184, 1
Warner, B. D. 2004, Minor Planet Bulletin, 31, 85
Warner, B. D. 2005a, Minor Planet Bulletin, 32, 90
Warner, B. D. 2005b, Minor Planet Bulletin, 32, 4
Warner, B. D. 2006a, Minor Planet Bulletin, 33, 58
Warner, B. D. 2006b, Minor Planet Bulletin, 33, 35
Warner, B. D. 2007, Minor Planet Bulletin, 34, 72
Warner, B. D. 2008a, Minor Planet Bulletin, 35, 56
Warner, B. D. 2008b, Minor Planet Bulletin, 35, 163
Warner, B. D. 2009a, Minor Planet Bulletin, 36, 109
Warner, B. D. 2009b, Minor Planet Bulletin, 36, 172
Warner, B. D. 2011a, Minor Planet Bulletin, 38, 52
Warner, B. D. 2011b, Minor Planet Bulletin, 38, 63
Warner, B. D. 2011c, Minor Planet Bulletin, 38, 96
Warner, B. D., Harris, A. W., & Pravec, P. 2009, Icarus, 202, 134
Yeung, K. W. 2006, Minor Planet Bulletin, 33, 49
Yoshida, F., Dermawan, B., Nakamura, T., et al. 2005, Abstr. IAU Symp., 229, 82

[1] Astronomical Institute, Faculty of Mathematics and Physics, Charles University in Prague, V Holešovičkách 2, 18000 Prague, Czech Republic
e-mail: hanus.home@gmail.com
[2] Astronomical Observatory Institute, Faculty of Physics, A. Mickiewicz University, Słoneczna 36, 60-286 Poznań, Poland
[3] Palmer Divide Observatory, 17995 Bakers Farm Rd., Colorado Springs, CO 80908, USA
[4] 4438 Organ Mesa Loop, Las Cruces, NM 88011, USA
[5] Goat Mountain Astronomical Research Station, 11355 Mount Johnson Court, Rancho Cucamonga, CA 91737, USA
[6] Geneva Observatory, 1290 Sauverny, Switzerland
[7] European Space Astronomy Centre, Spain, PO Box 78, 28691 Villanueva de la Cañada, Madrid, Spain
[8] Astronomical Institute of the Academy of Sciences, Fričova 298, 25165 Ondřejov, Czech Republic
[9] Observatoire de Bédoin, 47 rue Guillaume Puy, 84000 Avignon, France
[10] Observatoire de Chinon, Mairie de Chinon, 37500 Chinon, France
[11] Courbes de rotation d'astéroïdes et de comètes, CdR
[12] Association T60, 14 avenue Édouard Belin, 31400 Toulouse, France
[13] Harfleur, France
[14] Observatoire des Engarouines, 84570 Mallemort-du-Comtat, France
[15] Collonges Observatory, 90 allée des résidences, 74160 Collonges, France
[16] Paris and Saint-Savinien, France
[17] 139 Antibes, France
[18] Via M. Rosa, 1, 00012 Colleverde di Guidonia, Rome, Italy
[19] 947 Saint-Sulpice, France
[20] IMCCE – Paris Observatory – UMR 8028 CNRS, 77 Av. Denfert-Rochereau, 75014 Paris, France
[21] A90 San Gervasi, Spain
[22] l'Observatoire de Cabris, 408 chemin Saint Jean Pape, 06530 Cabris, France
[23] 929 Blackberry Observatory, USA
[24] Plateau du Moulin à Vent, St-Michel l'Observatoire, France
[25] J80 Saint-Hélène, France
[26] B13 Tradate, Italy
[27] 138 Village-Neuf, France
[28] TASS = The Amateur Sky Survey
[29] Shed of Science Observatory, 5213 Washburn Ave. S, Minneapolis, MN 55410, USA
[30] Association AstroQueyras, 05350 Saint-Véran, France
[31] Association des Utilisateurs de Détecteurs Électroniques (AUDE), France
[32] Observatoire du Bois de Bardon, 16110 Taponnat, France
[33] Dark Cosmology Centre, Niels Bohr Institute, University of Copenhagen, Juliane Maries Vej 30, 2100 Copenhagen, Denmark
[34] Nordic Optical Telescope, Apartado 474, 38700 Santa Cruz de La Palma, Santa Cruz de Tenerife, Spain
[35] Hamanowa Astronomical Observatory, Hikarigaoka 4–34, Motomiya, Fukushima, Japan

[36] Institute of Planetary Research, German Aerospace Center, Rutherfordstrasse 2, 12489, Berlin, Germany
[37] Hunters Hill Observatory, 7 Mawalan Street, Ngunnawal ACT 2913, Australia
[38] 056 Skalnaté Pleso, Slovakia
[39] A83 Jakokoski, Finland
[40] Astrophysics Division, Institute of Physics, Jan Kochanowski University, Świętokrzyska 15, 25–406 Kielce, Poland
[41] Université de Toulouse, UPS-OMP, IRAP, 31400 Toulouse, France
[42] CNRS, IRAP, 14 avenue Édouard Belin, 31400 Toulouse, France
[43] 980 Antelope Drive West, Bennett, CO 80102, USA
[44] LESIA-Observatoire de Paris, CNRS, UPMC Univ. Paris 06, Univ. Paris-Diderot, 5 place Jules Janssen, 92195 Meudon, France
[45] Stazione Astronomica di Sozzago, 28060 Sozzago, Italy
[46] Forte Software, Os. Jagiełły 28/28 60-694 Poznań, Poland
[47] SUPA (Scottish Universities Physics Alliance), Institute for Astronomy, University of Edinburgh, Royal Observatory, Edinburgh, EH9 3HJ, UK
[48] Club d'Astronomie Lyon Ampère, 37 rue Paul Cazeneuve, 69008 Lyon, France
[49] 174 Nyrölä, Finland
[50] Observatorio Montcabre, C/Jaume Balmes 24, 08348 Cabrils, Barcelona, Spain
[51] Observatori Astronómico de Mallorca, Camí de l'Observatori, s/n 07144 Costitx, Mallorca, Spain
[52] Kingsgrove, NSW, Australia
[53] Mt. Suhora Observatory, Pedagogical University, Podchorążych 2, 30-084, Cracow, Poland
[54] University of Helsinki, Department of Physics, PO Box 64, 00014 Helsinki
[55] Department of Earth, Atmospheric, and Planetary Sciences, Massachusetts Institute of Technology, Cambridge, MA 02139, USA
[56] 2 rue des Écoles, 34920 Le Crès, France
[57] F.-X. Bagnoud Observatory, 3961 St.-Luc, Switzerland
[58] Blauvac Observatory, 84570 St.-Estéve, France
[59] Observatoire de la Côte d'Azur, BP 4229, 06304 Nice Cedex 4, France
[60] Observatoire de Paris-Meudon, LESIA, 92190 Meudon, France
[61] 143 Gnosca, Switzerland
[62] DeKalb Observatory, 2507 CR 60, Auburn, IN 46706, USA
[63] 181 Les Makes, la Réunion, France
[64] CNRS-LKB-École Normale Supérieure – UMR 8552 – 24 rue Lhomond, 75005 Paris, France
[65] ANS Collaboration, c/o Osservatorio Astronomico di Padova, Sede di Asiago, 36032 Asiago (VI), Italy
[66] Institute of Astronomy, Karazin Kharkiv National University, Sums'ka 35, 61022 Kharkiv, Ukraine
[67] Observatoire Francois-Xavier Bagnoud, 3961 St.-Luc, Switzerland

Pages 11 to 16 are available in the electronic edition of the journal at http://www.aanda.org

Table 3. Observations used for the successful model determinations that are not included in the UAPC.

Asteroid	Date	Observer	Observatory (MPC code)
11 Parthenope	2008 5–2008 9	Warner	Palmer Divide Observatory (716)
	2008 7–2008 7	Pilcher[b]	Organ Mesa Observatory (G50)
	2009 11–2010 1	Pilcher (2010)	
	2011 2–2011 5	Pilcher (2011a)	
	2011 3–2011 3	Audejean	Observatoire de Chinon, France (B92)
	2011 4–2011 4	Naves	Observatorio Montcabre (213)
25 Phocaea	2006 10–2006 10	Buchheim	Altimira Observatory, USA (G76)
	2006 10 21.9	Strajnic, Grangeon, Coupier, Godon, Roche Danavaro, Dalmas, Bayol, Behrend	Haute-Provence Observatory, France (511)
	2008 1–2009 4	Pilcher (2009a)	
	2010 9–2010 12	Pilcher (2011b)	
72 Feronia	2004 3–2004 4	Bernasconi	Les Engarouines Observatory, France (A14)
	2005 7–2005 8	Bernasconi	Les Engarouines Observatory, France (A14)
	2007 1 20.9	Coliac	Observatoire Farigourette, France
	2011 3–2011 4	Marciniak	Borowiec, Poland (187)
	2011 5 9.9	Hirsch	Borowiec, Poland (187)
147 Protogeneia	2004 11–2004 12	Buchheim (2005)	
	2005 1 4.9	Roy	Blauvac Observatory, France (627)
	2005 1–2005 1	Bernasconi	Les Engarouines Observatory, France (A14)
	2008 5 29.7	Higgins[a]	Hunters Hill Observatory, Ngunnawal (E14)
149 Medusa	2010 10–2010 11	Pilcher (2011b)	
	2010 11–2010 12	Martin	Tzec Maun Observatory, Mayhill (H10)
157 Dejanira	2005 3–2005 3	Poncy	Le Crés, France (177)
	2005 4–2005 5	Warner (2005a)	
	2008 12–2009 2	Pilcher (2009c)	
166 Rhodope	2010 12–2011 1	Conjat	Cabris, France
178 Belisana	2007 4-2007 7	Oey & Krajewski (2008)	
	2008 9–2008 10	Pilcher et al. (2009)	
183 Istria	2004 2 14.1	Bernasconi	Les Engarouines Observatory, France (A14)
193 Ambrosia	2009 4–2009 4	Warner (2009b)	
	1999 10 15.0	Hirsch	Borowiec, Poland (187)
	2005 4–2005 4	Kaminski	Borowiec, Poland (187)
	2005 4 3.9	Marciniak	Borowiec, Poland (187)
	2005 4–2005 4	Hirsch	Borowiec, Poland (187)
	2009 3–2009 3	Audejean	Observatoire de Chinon, France (B92)
	2009 4–2009 5	Hirsch	Borowiec, Poland (187)
	2009 4 29.9	Kaminski	Borowiec, Poland (187)
	2010 4 19.1	Borczyk	SAAO, Sutherland, South Africa
199 Byblis	2003 3–2003 4	Casulli	Vallemare di Bordona, Italy (A55)
	2003 5–2003 5	Bernasconi	Les Engarouines Observatory, France (A14)
	2005 10–2005 10	Roy	Blauvac Observatory, France (627)
	2005 10–2005 10	Casulli	Vallemare di Bordona, Italy (A55)
	2005 11–2005 11	Stoss, Nomen, Sanchez, Behrend	OAM, Mallorca (620)
	2005 11 20.9	Farroni	
	2006 12–2006 12	Roy	Blauvac Observatory, France (627)
	2008 2 9.1	Manzini	Stazione Astronomica di Sozzago, Italy (A12)
	2011 9 24.1	Sobkowiak	Borowiec, Poland (187)
	2011 11–2011 11	Marciniak	Borowiec, Poland (187)
220 Stephania	2004 10–2004 10	Koff	Antelope Hills Observatory, Bennett (H09)
222 Lucia	1999 4 18.2	Warner	Palmer Divide Observatory (716)
	2008 12–2008 12	Stephens (2009a)	
	2010 4–2010 5	Audejean	Observatoire de Chinon, France (B92)
	2010 4–2010 4	Bosch	Collonges Observatory, France (178)
242 Kriemhild	2004 7–2004 7	Bosch	Collonges Observatory, France (178)
	2004 8–2004 8	Warner (2005b)	
	2004 9–2004 9	Rinner	Ottmarsheim Observatory, France (224)
	2005 11 7.9	Roy	Blauvac Observatory, France (627)
	2007 1–2007 1	Bembrick et al. (2007)	
	2009 8–2009 8	Audejean	Observatoire de Chinon, France (B92)
	2010 8–2011 3	Marciniak	Borowiec, Poland (187)
	2010 10 10.1	T. Michałowski	Borowiec, Poland (187)
	2011 11–2012 1	Marciniak	Borowiec, Poland (187)
	2011 11 13.1	Sobkowiak	Borowiec, Poland (187)

Notes. [(a)] On line at `http://www.david-higgins.com/Astronomy/asteroid/lightcurves.htm`; [(b)] On line at `http://aslc-nm.org/Pilcher.html`; [(c)] Observations, reductions, and calibration methods are described in Polishook & Brosch (2008, 2009).

Table 3. continued.

Asteroid	Date	Observer	Observatory (MPC code)
257 Silesia	2004 12–2004 12	Casulli, Behrend	Vallemare di Bordona, Italy (A55)
	2004 12–2005 1	Roy	Blauvac Observatory, France (627)
	2005 1 31.1	Starkey	DeKalb Observatory, USA (H63)
	2005 12 1.1	Strajnic, Paulo, Wagrez, Jade, Rocca, Del Freo, Behrend	Haute-Provence Observatory, France (511)
	2005 12–2006 1	Roy	Blauvac Observatory, France (627)
	2005 12–2005 12	Antonini	Observatoire de Bédoin, France (132)
260 Huberta	2005 3–2005 3	Roy	Blauvac Observatory, France (627)
	2007 7–2007 8	Roy	Blauvac Observatory, France (627)
272 Antonia	2007 12–2008 1	Pilcher (2008)	
	2011 10–2011 10	S. Fauvaud, M. Fauvaud	Observatoire du Bois de Bardon, France
281 Lucretia	2011 10–2011 10	S.Fauvaud, M. Fauvaud	Observatoire du Bois de Bardon, France
290 Bruna	2008 3–2008 4	Pilcher (2009b)	
297 Caecilia	2004 11–2004 12	Roy	Blauvac Observatory, France (627)
	2006 1–2006 1	Manzini	Stazione Astronomica di Sozzago, Italy (A12)
	2006 1 11.0	Antonini	Observatoire de Bédoin, France (132)
	2006 1 13.1	Roy	Blauvac Observatory, France (627)
	2009 12 11.8	Salom, Esteban	Caimari (B81)
	2011 2–2011 3	Marciniak	Borowiec, Poland (187)
	2012 1 30.2	Marciniak	Borowiec, Poland (187)
	2012 1 31.2	Polinska	Borowiec, Poland (187)
	2012 2–2012 3	Hirsch	Borowiec, Poland (187)
345 Tercidina	2002 9–2002 10	Barbotin	Villefagnan Observatory, France
	2002 9–2002 12	Bernasconi	Les Engarouines Observatory, France (A14)
	2002 9–2002 10	Rinner	Ottmarsheim Observatory, France (224)
	2002 9–2002 9	Starkey, Bernasconi	Les Engarouines Observatory, France (A14)
	2002 9–2002 9	Waelchli, Revaz	F.-X. Bagnoud Observatory, Switzerland (175)
	2002 10 1.1	Michelet	
	2002 10 5.2	Barbotin	Villefagnan Observatory, France
	2002 11 22.9	Bosch	Collonges Observatory, France (178)
	2002 11-2002 12	Starkey	DeKalb Observatory, USA (H63)
	2004 4–2004 5	Bernasconi	Les Engarouines Observatory, France (A14)
	2004 4–2004 5	Roy	Blauvac Observatory, France (627)
	2005 8–2005 8	Bernasconi	Les Engarouines Observatory, France (A14)
	2005 8 27.0	Stoss, Nomen, Sanchez, Behrend	OAM, Mallorca (620)
	2005 9 8.0	Farroni	
	2008 7 5.0	Trégon, Leroy	Pic du Midi Observatory (586)
	2009 8–2009 10	Naves	Observatorio Montcabre (213)
	2011 4 22.9	Sobkowiak	Borowiec, Poland (187)
352 Gisela	2002 10 8.7	Droege	
	2004 2 13.1	Bernasconi, Klotz, Behrend	Haute-Provence Observatory, France (511)
	2005 7–2005 8	Bernasconi	Les Engarouines Observatory, France (A14)
371 Bohemia	2001 6–2004 3	Buchheim et al. (2004)	
	2006 9 2.0	Bernasconi	Les Engarouines Observatory, France (A14)
	2011 8–2011 11	Marciniak	Borowiec, Poland (187)
	2011 11 2.9	W. Ogłoza	Mnt. Suhora, Poland
	2011 11 30.9	Santana-Ros	Borowiec, Poland (187)
390 Alma	2004 8–2004 8	Stephens (2005b)	
	2008 8–2008 10	Roy	Blauvac Observatory, France (627)
403 Cyane	2001 12 9.1	Brunetto	Le Florian, France (139)
	2001 12–2001 12	Bernasconi	Les Engarouines Observatory, France (A14)
	2001 12 22.2	Cooney	
	2005 10 1.0	Bernasconi	Les Engarouines Observatory, France (A14)
	2007 2–2007 2	Roy	Blauvac Observatory, France (627)
404 Arsinoe	1999 3–1999 4	Kryszczynska	Borowiec, Poland (187)
	1999 3 19.0	Hirsch	Borowiec, Poland (187)
	1999 3 20.0	T. Michałowski	Borowiec, Poland (187)
	2001 10–2001 10	S. Fauvaud, Heck, Santacana, Wucher	Pic de Château-Renard Observatory
	2001 11–2001 12	Bernasconi	Les Engarouines Observatory, France (A14)
	2003 4–2003 4	Roy	Blauvac Observatory, France (627)
	2005 8 10.1	Fagas	Borowiec, Poland (187)
	2005 10–2005 10	Hirsch	Borowiec, Poland (187)
	2005 10–2005 11	Roy	Blauvac Observatory, France (627)
	2006 11–2007 1	Fagas	Borowiec, Poland (187)
	2007 1–2007 4	Marciniak	Borowiec, Poland (187)
	2007 2 17.0	Hirsch	Borowiec, Poland (187)

Table 3. continued.

Asteroid	Date	Observer	Observatory (MPC code)
	2007 4–2007 4	Kaminski	Borowiec, Poland (187)
	2007 4 22.0	Kankiewicz	Kielce, Poland (B02)
	2008 6–2008 6	Marciniak	SAAO, Sutherland, South Africa
	2009 8–2009 10	Marciniak	SAAO, Sutherland, South Africa
	2009 9 27.0	Hirsch	Borowiec, Poland (187)
	2009 10 30.0	Polinska	Borowiec, Poland (187)
	2009 12 3.0	Kaminski	Borowiec, Poland (187)
	2010 12 5.0	Sobkowiak	Borowiec, Poland (187)
	2011 1–2011 5	Marciniak	Borowiec, Poland (187)
	2011 3–2011 3	Hirsch	Borowiec, Poland (187)
406 Erna	2005 9–2005 10	Casulli	Vallemare di Bordona, Italy (A55)
	2005 11–2005 11	Crippa, Manzini	Stazione Astronomica di Sozzago, Italy (A12)
	2005 11–2005 11	Poncy	Le Crés, France (177)
441 Bathilde	2003 1–2003 1	Roy	Blauvac Observatory, France (627)
	2003 2–2003 2	Bernasconi	Les Engarouines Observatory, France (A14)
	2003 2–2003 3	Vagnozzi, Cristofanelli, Paiella	Santa Lucia Stroncone (589)
	2005 7–2005 8	Bernasconi	Les Engarouines Observatory, France (A14)
	2006 12 11.9	Poncy	Le Crés, France (177)
	2010 9–2010 10	Marciniak	Borowiec, Poland (187)
	2010 10 4.8	Kaminski	Borowiec, Poland (187)
	2010 10 9.9	T. Michałowski	Borowiec, Poland (187)
	2011 10 14.0	Sobkowiak	Borowiec, Poland (187)
	2011 10–2011 11	Marciniak	Borowiec, Poland (187)
507 Laodica	2001 8–2001 8	Charbonnel	Durtal (949)
	2001 8–2001 9	Leyrat	
509 Iolanda	1996 10–1996 10	López-González & Rodríguez (2000)	
	2000 6 8.3	Koff & Brincat (2000)	
512 Taurinensis	2004 12–2005 1	Poncy	Le Crés, France (177)
	2005 1 5.0	Correia	Haute-Provence Observatory, France (511)
528 Rezia	2011 3–2011 3	Mottola	
531 Zerlina	2002 6 2.9	Christophe	
	2007 9–2007 10	Brinsfield (2008b)	
	2011 3–2011 6	Pilcher & Brinsfield (2011)	
543 Charlotte	2006 11–2006 12	Poncy	Le Crés, France (177)
572 Rebekka	2007 2–2007 2	Warner (2007)	
	2009 8–2009 8	Audejean	Observatoire de Chinon, France (B92)
578 Happelia	2006 12–2006 12	Leroy	Uranoscope, France (A07)
	2008 4–2008 4	Warner (2008b)	
	2010 11–2010 12	Antonini	Observatoire de Bédoin, France (132)
	2012 2–2012 4	Mottola, Hellmich	
600 Musa	2001 4 6.0	Hirsch	Borowiec, Poland (187)
	2001 4 29.0	Colas	Pic du Midi Observatory (586)
	2005 2–2005 3	Bernasconi	Les Engarouines Observatory, France (A14)
	2005 3–2005 4	Hirsch	Borowiec, Poland (187)
	2005 4 1.0	Marciniak	Borowiec, Poland (187)
	2007 10–2007 10	S. Fauvaud, Santacana, M. Fauvaud	Pic du Midi Observatory (586)
	2009 3 25.8	Kaminski	Borowiec, Poland (187)
	2009 3 30.9	Marciniak	Borowiec, Poland (187)
	2010 4–2010 6	Marciniak	Borowiec, Poland (187)
	2011 11–2011 11	Marciniak	Borowiec, Poland (187)
	2011 11 29.8	Hirsch	Borowiec, Poland (187)
669 Kypria	2006 3–2006 4	Bernasconi	Les Engarouines Observatory, France (A14)
708 Raphaela	2007 2–2007 2	Warner (2007)	
725 Amanda	2002 12 12.8	Marciniak	Borowiec, Poland (187)
	2002 12 31.8	T. Michałowski	Borowiec, Poland (187)
	2006 10–2006 10	S. Fauvaud, Santacana, Sareyan, Wucher	Pic de Château-Renard Observatory
	2006 10 30.1	Hirsch	Borowiec, Poland (187)
	2009 8–2009 8	Marciniak	SAAO, Sutherland, South Africa
	2010 10–2010 10	Audejean	Observatoire de Chinon, France (B92)
	2010 10 31.0	Marciniak	Borowiec, Poland (187)
	2012 3 3.1	Marciniak	Borowiec, Poland (187)
	2012 3–2012 3	Hirsch	Borowiec, Poland (187)
	2012 4 10.1	Oszkiewicz, Geier	NOT, La Palma, Canary Islands
731 Sorga	2005 4–2005 4	Warner (2005a)	
	2009 2–2009 2	Warner (2009a)	
732 Tjilaki	2004 3–2004 4	Bernasconi	Les Engarouines Observatory, France (A14)
787 Moskva	1999 5–1999 5	Warner (2011a)	

Table 3. continued.

Asteroid	Date	Observer	Observatory (MPC code)
	2003 4–2003 5	Husarik, Behrend	Skalnate Pleso, Slovakia (056)
	2003 5–2003 5	Bernasconi	Les Engarouines Observatory, France (A14)
	2004 8–2004 8	Bernasconi	Les Engarouines Observatory, France (A14)
	2011 5–2011 5	Audejean	Observatoire de Chinon, France (B92)
	2011 5–2011 5	Morelle	Observatoire Farigourette, France
792 Metcalfa	2010 7–2010 8	Roy	Blauvac Observatory, France (627)
803 Picka	2006 12 10.8	Bosch	Collonges Observatory, France (178)
	2007 4–2007 4	Antonini	Observatoire de Bédoin, France (132)
	2010 11–2010 11	Antonini	Observatoire de Bédoin, France (132)
812 Adele	2002 10–2002 10	Roy	Blauvac Observatory, France (627)
816 Juliana	2005 4–2005 4	Stephens (2005a)	
	2005 5–2005 6	Conjat	Cabris, France
	2010 3–2010 3	Conjat	Cabris, France
852 Wladilena	2003 2 23.2	J. Michałowski	Borowiec, Poland (187)
	2003 2 24.2	Marciniak	Borowiec, Poland (187)
	2003 2 26.2	T. Michałowski	Borowiec, Poland (187)
	2007 5–2007 5	Marciniak	SAAO, Sutherland, South Africa
	2008 8 22.2	M. J. Michałowski	NOT, La Palma, Canary Islands
	2008 10–2009 1	Kaminski	Borowiec, Poland (187)
	2008 9–2008 10	Marciniak	Borowiec, Poland (187)
	2008 12–2009 1	Sobkowiak	Borowiec, Poland (187)
	2010 2–2010 3	Antonini	Observatoire de Bédoin, France (132)
	2010 3–2010 5	Marciniak	Borowiec, Poland (187)
	2010 3–2010 3	Polishook (2012)[c]	Wise Observatory, Mitzpeh Ramon (097)
	2010 3–2010 4	Sobkowiak	Borowiec, Poland (187)
857 Glasenapia	2006 12 23.0	Poncy	Le Crés, France (177)
867 Kovacia	2006 11 22.8	Crippa, Manzini	Stazione Astronomica di Sozzago, Italy (A12)
	2008 1–2008 2	Roy	Blauvac Observatory, France (627)
	2008 2 8.9	Casulli	Vallemare di Bordona, Italy (A55)
	2008 2 9.0	Colas	Pic du Midi Observatory (586)
	2008 2–2008 2	Manzini	Stazione Astronomica di Sozzago, Italy (A12)
	2008 2–2008 2	Leroy	Uranoscope, France (A07)
	2008 2–2008 2	Demeautis	Village-Neuf Observatory, France (138)
	2008 2–2008 3	Coliac	Observatoire Farigourette, France
874 Rotraut	2002 7–2002 7	Charbonnel	Durtal (949)
	2002 8 16.0	Rinner	Ottmarsheim Observatory, France (224)
875 Nymphe	2003 7–2003 7	Warner (2011c)	
	2003 7–2003 7	Roy	Blauvac Observatory, France (627)
900 Rosalinde	2007 5 19.0	Roy	Blauvac Observatory, France (627)
994 Otthild	2001 9 22.0	Velichko, T. Michałowski	Kharkov (101)
	2001 10–2001 10	J. Michałowski	Borowiec, Poland (187)
	2001 10–2001 10	Conjat	Cabris, France
	2001 11–2001 11	T. Michałowski	Borowiec, Poland (187)
	2001 11–2001 11	Kwiatkowski	Borowiec, Poland (187)
	2005 8–2005 11	Stoss, Nomen, Sanchez, Behrend	OAM, Mallorca (620)
	2005 10 1.9	Bernasconi	Les Engarouines Observatory, France (A14)
	2005 10–2005 10	Fagas	Borowiec, Poland (187)
	2005 10 19.9	T. Michałowski	Borowiec, Poland (187)
	2007 2 26.9	S. Fauvaud, Esseiva, Michelet, Saguin, Sareyan	Pic de Château-Renard Observatory
	2011 3 19.9	Polinska	Borowiec, Poland (187)
	2011 3 29.8	Marciniak	Borowiec, Poland (187)
1056 Azalea	2004 2–2004 2	Klotz, Behrend	Haute-Provence Observatory, France (511)
1089 Tama	2003 12–2004 3	Roy	Blauvac Observatory, France (627)
	2003 12–2004 2	Rinner	Ottmarsheim Observatory, France (224)
	2004 1–2004 1	Antonini	Observatoire de Bédoin, France (132)
	2004 1–2004 1	Sposetti, Behrend	Gnosca Observatory, Switzerland (143)
	2004 1 4.9	Klotz	Haute-Provence Observatory, France (511)
	2004 1–2004 1	Lecacheux, Colas	Pic du Midi Observatory (586)
	2004 1 22.8	Colas	Pic du Midi Observatory (586)
	2004 1 26.9	Michelsen, Augustesen, Masi	Brorfelde (054)
	2004 1–2004 1	Cotrez, Behrend	Saint-Hélène Observatory, France (J80)
	2004 1–2004 2	Durkee	Shed of Science Observatory, USA (H39)
	2004 2 7.9	Bernasconi	Les Engarouines Observatory, France (A14)
	2004 2 9.8	Coloma	Sabadell (619)
	2004 2–2004 2	Oksanen	Nyrölä Observatory, Finland (174)
	2004 2 11.9	Itkonen, Pääkkönen	Jakokoski Observatory, Finland (A83)

Table 3. continued.

Asteroid	Date	Observer	Observatory (MPC code)
	2004 2 15.0	Brochard	
	2004 2 20.9	Demeautis, Matter	Village-Neuf Observatory, France (138)
	2004 2 24.1	Barbotin, Cotrez, Cazenave, Laffont	Pic du Midi Observatory (586)
	2005 6–2005 7	Stoss, Nomen, Sanchez, Behrend	OAM, Mallorca (620)
	2005 7–2005 8	Teng, Behrend	Observatoire Les Makes, France (181)
	2006 9–2006 12	Sposetti, Pavic	Gnosca Observatory, Switzerland (143)
	2006 9–2006 12	Polishook (2012)[c]	Wise Observatory, Mitzpeh Ramon (097)
	2006 11 26.9	Sposetti, Behrend	Gnosca Observatory, Switzerland (143)
	2008 4 5.1	Klotz, Strajnic	Haute-Provence Observatory, France (511)
	2008 5–2008 5	Roy	Blauvac Observatory, France (627)
	2008 5–2008 5	Polishook (2012)[c]	Wise Observatory, Mitzpeh Ramon (097)
	2009 10–2009 11	Polishook (2012)[c]	Wise Observatory, Mitzpeh Ramon (097)
	2011 2–2011 3	Crippa, Manzini	Stazione Astronomica di Sozzago, Italy (A12)
1111 Reinmuthia	2007 10–2007 11	Hiromi Hamanowa, Hiroko Hamanowa	
1126 Otero	2008 2–2008 2	Stephens (2008)	
1130 Skuld	2004 1 22.0	Colas	Pic du Midi Observatory (586)
	2009 10–2009 11	Buchheim (2010)	
1188 Gothlandia	2006 1 2.9	Pallares	Sabadell (619)
	2006 1 11.9	Coloma	Agrupación Astronómica de Sabadell, Spain (A90)
	2006 2 2.9	Coloma, Garcia	Agrupación Astronómica de Sabadell, Spain (A90)
	2007 5–2007 5	Antonini	Observatoire de Bédoin, France (132)
	2008 12–2009 1	H. Hamanowa, H. Hamanowa	
	2011 8–2011 12	Baker et al. (2012)	
	2011 9–2011 9	S. Fauvaud, M. Fauvaud	Observatoire du Bois de Bardon, France
1241 Dysona	2002 9–2002 11	Bosch	Collonges Observatory, France (178)
	2002 10 2.0	Brunetto	Le Florian, France (139)
	2006 4–2006 5	Oey	Leura (E17)
1249 Rutherfordia	2001 8–2001 8	Bernasconi	Les Engarouines Observatory, France (A14)
	2008 8 22.0	Demeautis	Village-Neuf Observatory, France (138)
	2004 7–2004 7	Roy	Blauvac Observatory, France (627)
1317 Silvretta	2006 4–2006 4	Bernasconi	Les Engarouines Observatory, France (A14)
	2009 12–2010 1	Ruthroff (2010)	
1386 Storeria	2004 6–2004 6	Warner (2004)	
	2004 7 15.0	Behrend, Klotz	Haute-Provence Observatory, France (511)
	2004 7 17.0	Bernasconi	Les Engarouines Observatory, France (A14)
	2004 7 21.0	Coloma	Agrupación Astronómica de Sabadell, Spain (A90)
	2004 7 28.0	Roy	Blauvac Observatory, France (627)
1401 Lavonne	2008 8 8.3	Durkee	Shed of Science Observatory, USA (H39)
	2008 9–2008 9	Antonini	Observatoire de Bédoin, France (132)
1432 Ethiopia	2007 7–2007 9	Oey (2008)	
1436 Salonta	2007 8–2007 9	Warner (2008a)	
	2007 10–2007 10	Antonini	Observatoire de Bédoin, France (132)
	2008 11–2008 11	Antonini	Observatoire de Bédoin, France (132)
	2008 11 27.8	Roy	Blauvac Observatory, France (627)
1472 Muonio	2008 9–2008 9	Stephens (2009b)	
	2008 10–2008 10	Higgins[a]	Hunters Hill Observatory, Ngunnawal (E14)
1490 Limpopo	2005 8–2005 8	Bernasconi	Les Engarouines Observatory, France (A14)
1495 Helsinki	2006 4–2006 5	Oey et al. (2007)	
	2006 6 4.0	Payet, Teng, Leonie, Behrend	Observatoire Les Makes, France (181)
	2006 6–2006 7	Teng, Behrend	Observatoire Les Makes, France (181)
	2011 9–2011 9	S. Fauvaud, M. Fauvaud	Observatoire du Bois de Bardon, France
1518 Rovaniemi	2009 1–2009 1	Warner (2009a)	
	2009 1–2009 1	Roy	Blauvac Observatory, France (627)
1528 Conrada	2008 5–2008 5	Warner (2008b)	
1554 Yugoslavia	2007 4–2007 4	Higgins (2008)	
1559 Kustaanheimo	2005 3–2005 3	Bernasconi	Les Engarouines Observatory, France (A14)
1572 Posnania	1993 9–1999 11	Michałowski et al. (2001)	
	2004 9–2004 9	Roy	Borowiec, Poland (187)
	2010 12 5.1	Sobkowiak	Borowiec, Poland (187)
	2011 2–2011 2	Kaminski	Borowiec, Poland (187)
	2011 2 8.8	Marciniak	Borowiec, Poland (187)
	2012 2–2012 3	Roy	Blauvac Observatory, France (627)
1607 Mavis	2007 9–2007 9	Oey (2008)	
1630 Milet	2005 2–2005 2	Bernasconi	Les Engarouines Observatory, France (A14)
1634 Ndola	2006 9–2006 9	Higgins[a]	Hunters Hill Observatory, Ngunnawal (E14)
1719 Jens	2000 9–2000 9	Warner (2011b)	
	2006 1–2006 2	Bernasconi	Les Engarouines Observatory, France (A14)

Table 3. continued.

Asteroid	Date	Observer	Observatory (MPC code)
1785 Wurm	2008 3–2008 3	Oey (2009)	
1837 Osita	2006 1–2006 3	Roy	Blauvac Observatory, France (627)
1927 Suvanto	2005 2–2005 2	Bernasconi	Les Engarouines Observatory, France (A14)
1933 Tinchen	2005 3 14.0	Roy	Blauvac Observatory, France (627)
1950 Wempe	2006 2 1.9	Bernasconi	Les Engarouines Observatory, France (A14)
1963 Bezovec	2005 1–2005 1	Bernasconi	Les Engarouines Observatory, France (A14)
	2009 3–2009 3	Romeuf	
	2009 4 6.9	Manzini	Stazione Astronomica di Sozzago, Italy (A12)
	2009 4–2009 4	Martin	Tzec Maun Observatory, Mayhill (H10)
2002 Euler	2006 5–2006 5	Koff	Antelope Hills Observatory, Bennett (H09)
	2007 10–2007 10	Higgins[a]	Hunters Hill Observatory, Ngunnawal (E14)
2510 Shandong	2006 8–2006 9	Higgins & Goncalves (2007)	
2606 Odessa	2008 2–2008 2	Higgins et al. (2008)	
	2008 3 3.6	Oey	Leura (E17)
2709 Sagan	2008 3–2008 3	Higgins et al. (2008)	
	2011 1–2011 2	Oey	Leura (E17)
2839 Annette	2005 10–2005 11	Buchheim (2007)	
	2005 12–2005 12	Warner (2006a)	
2957 Tatsuo	2005 8–2005 8	Bernasconi	Les Engarouines Observatory, France (A14)
	2005 8–2005 9	Poncy	Le Crés, France (177)
	2005 9–2005 9	Warner (2006b)	
2991 Bilbo	2007 4–2007 4	Higgins[a]	Hunters Hill Observatory, Ngunnawal (E14)
3722 Urata	2004 12–2004 12	Antonini	Observatoire de Bédoin, France (132)
	2006 9 3.0	Manzini	Stazione Astronomica di Sozzago, Italy (A12)
	2007 8–2007 8	Roy	Blauvac Observatory, France (627)
	2007 8–2007 8	Stephens	Goat Mountain Astronomical Research Station (G79)
5281 Lindstrom	2008 6–2008 6	Brinsfield	Via Capote Sky Observatory, Thousand Oaks (G69)
7517 1989 AD	2007 11–2007 11	Stephens	Goat Mountain Astronomical Research Station (G79)
8132 Vitginzburg	2008 6–2008 6	Brinsfield (2008a)	
8359 1989 WD	2009 4–2009 4	Higgins & Warner (2009)	
	2009 5–2009 5	Brinsfield (2009)	
10772 1990 YM	2006 3–2006 3	Koff	Antelope Hills Observatory, Bennett (H09)
	2006 4–2006 4	Warner	Palmer Divide Observatory (716)
31383 1998 XJ_{94}	2006 4–2006 4	Higgins et al. (2006)	